Cytometry 7:467–474 (1986)

# Characterization of Chromatin Distribution in Cell Nuclei

**Ian T. Young, P.W. Verbeek, and Brian H. Mayall**

Pattern Recognition Group, Department of Applied Physics, Delft University of Technology, 2600 GA Delft, The Netherlands (I.T.Y., P.W.V.) and Biomedical Sciences Division, Lawrence Livermore National Laboratory, University of California, Livermore, California 94550 (B.H.M.)

Received for publication July 18, 1985; accepted April 7, 1986

**In this paper we develop four measures to describe the distribution of nuclear chromatin. These measures attempt to describe in an objective and meaningful way the heterogeneity, granularity, condensation, and margination of chromatin in cell nuclei. Starting with a high-resolution digitized image of a cell where the nuclear pixels have been identified, the four measures may be rapidly estimated. The range of each is derived and the interpretation of the measures in the context of chromatin compaction and distribution is developed. Implementation issues such as sampling density, thresholding and subsequent pre-processing, and algorithmic complexity are discussed.**

**Key terms: Quantitative microscopy, image processing, texture measures, pattern recognition, image measurement**

In this paper we present four measures that we have developed to quantify and characterize the distribution of chromatin in the nuclei of stained cells. These measures are based upon a simple model for the way chromatin compacts in a cell nucleus and how that compaction is reflected in verbal descriptions of nuclear "texture." Use of the word texture immediately suggests a range of possibilities for quantification and it is not our purpose here to go into a lengthy review of the texture literature. What has guided us in this study, however, has been a search for ways of describing chromatin distribution that clearly relate to the underlying processes that cause change in the appearance of cell nuclei. Thus we start from a somewhat different perspective then the mathematical texture parameters of Haralick (5), Galloway (2), or Pressman (16).

## METHODS

### Modeling

We begin with the idea that a cell nucleus (as pictured in Figs. 1A,B) has a constant amount of DNA except when the cell is synthesizing DNA or about to divide.

Thus we are considering cells with a normal, diploid (2c) DNA content—G0 and G1 cells. In a typical cell population such cells will account for at least 85% of all randomly sampled cells (14). It is precisely these cells that we are interested in characterising with respect to chromatin distribution; cells with a DNA complement above the 2c level are easily found by measuring their DNA content.

If a difference exists between the nuclear chromatin pattern in two similar cells, then, according to our model of constant DNA, it must be due to a redistribution of the chromatin within the nucleus. This is illustrated in Figure 2A–D where all four cell images have precisely the same total nuclear optical density (proportional to DNA) but the distributions have been artificially altered.

We describe the possible chromatin variations in terms of three linguistic attributes: heterogeneity, granularity, and margination. The first, heterogeneity, refers to whether the nuclear chromatin is homogeneously distributed throughout the nucleus or condensed into granules.

If the chromatin is condensed, then the description of granularity assumes a useful role. While Figures 2C and D both exhibit an artificial granularity, the size of the "granules" differs significantly. Our granularity measures estimate the size distribution through a sieving technique. The final measure, margination, is based upon the observation that, in a number of biologically and clinically important situations, the chromatin density is distributed primarily around the nuclear membrane or margin with clearing towards the center of the nucleus.

Whether the margination exists in the (true) three-dimensional cell or is an effect that is visualized through the two-dimensional preparation technique is not clear. What is clear is that margination is a relevant indicator of the state of cell in certain disease processes.

Address reprint requests to Dr. I.T. Young, Pattern Recognition Group, Department of applied Physics, Loventzweg 1, Delft University of Technology, 2600 GA Delft, The Netherlands.

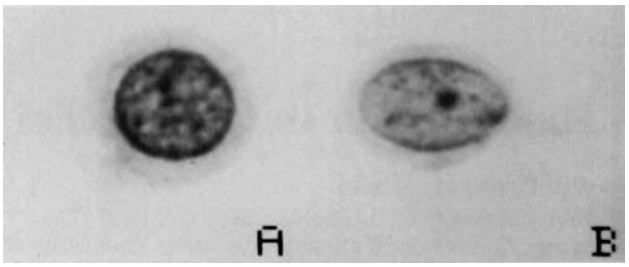


FIG. 1. Examples of cell nuclei with similar total DNA content but differing chromatin distribution.

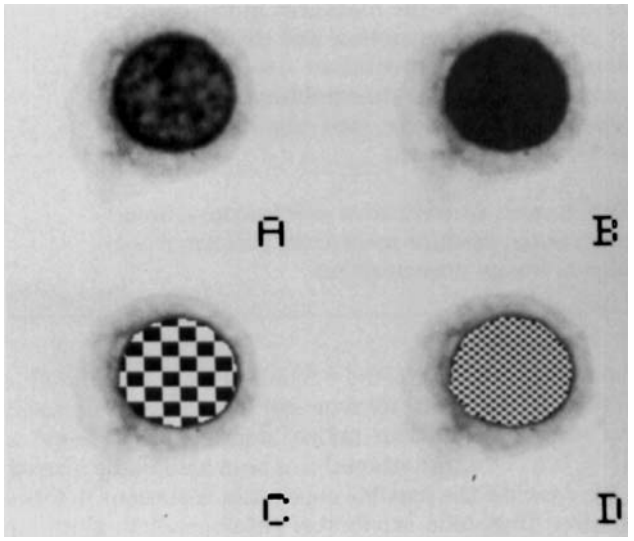


FIG. 2. A) Dissociated rat bladder cell (original); B) the same cell but with all nuclear pixels having the same average optical density as that in (A) thus producing a homogeneous nucleus; C) the same total optical density as in (A) and (B) but with a coarse "granulation"; D) the same as C) but with a fine "granulation."

## Chromatin Condensation—Heterogeneity and Granularity

Our technique for measuring the heterogeneity and granularity uses a preprocessing step that converts the grey-valued nuclear image (with normally 256 possible grey levels) into a three-level image where each level is, in fact, a label. For pixels within the nucleus, where the chromatin is highly compacted and thus very dark, we replace their values with grey value zero, that is BLACK. Where the chromatin has "cleared" we replace the value with 255, that is WHITE. Finally, where the chromatin remains approximately equal to the average value in the nucleus, the values are replaced with 128, GREY.

The differentiation between cleared regions, compacted regions, and average regions is based upon thresholds determined from the histogram of grey values within *each* cell nucleus. Such a histogram is shown in Figure 3 with the mean grey value and the two threshold levels indicated.

Program 1
*Short Version of a Program to Reassign Grey Values of Pixels Inside the Nucleus of a Cell. The Variables "Mean" and "Percentage" are Defined in the Text*

```
thresh1 = (1.0 − percent) * mean
thresh2 = (1.0 + percent) * mean
for (all pixels in nucleus n[x,y] )
  {
  if ( n[x,y] < thresh1 ) n[x,y] = BLACK;
  if ( n[x,y] >= thresh1 )
    {
    if ( n[x,y] < thresh2 ) n[x,y] = GREY;
    if ( n[x,y] >  = thresh 2 ) n[x,y] = WHITE;
    }
  }
```

The labeling then proceeds as shown in Program 1. First the mean grey value of all the pixels in the nucleus is computed. Then a fixed percentage is used to determine two thresholds — one above the mean and one below the mean. In the example of Figure 3 this percentage is 20% so that the two thresholds are 120% of the mean and 80% of the mean. The exact choice of the percentage is dependent upon the problem. At the very least it should be equal to or greater than the CV (coefficient-of-variation) of the system for measurement of either optical density or DNA. That is, if the measurement system gives a 3% CV for DNA measures on the 2c peak, then the percentage used in the computation of the thresholds should be at least 3%. This is in keeping with our model of DNA compaction described earlier.

Using percentages of the mean (instead of a fixed offset relative to the mean) means that our results will be invariant to multiplicative changes, for example, changes in the overall illumination level.

With the pixels in the nucleus reassigned, the nucleus now appears as is shown in Figure 4.

Based upon the labeled nuclear image we are now ready to define measures for nuclear heterogeneity and granularity. If the number of pixels in the nucleus labeled BLACK is $N_B$, the number labeled GREY is $N_G$, and the number labeled WHITE is $N_W$ then the heterogeneity measure (*hetero*) is defined by the dimensionless ratio:

$$\text{hetero} = \frac{N_B + N_W}{N_B + N_G + N_W}. \qquad (1)$$

A uniformly grey nucleus with no chromatin compaction will yield a value for *hetero* of 0.0 while a completely condensed nucleus, with all pixels either black or white, will yield a value of 1.0. Three observations can be made concerning this heterogeneity measure. First, the denominator in the definition is simply the total number of pixels in the nucleus, that is, the nuclear area. Second, the parameter itself may be computed directly from the histogram of nuclear values without reference to the original image. In other words, *hetero* may be computed from the histogram in Figure 3. Finally, if a homogene-

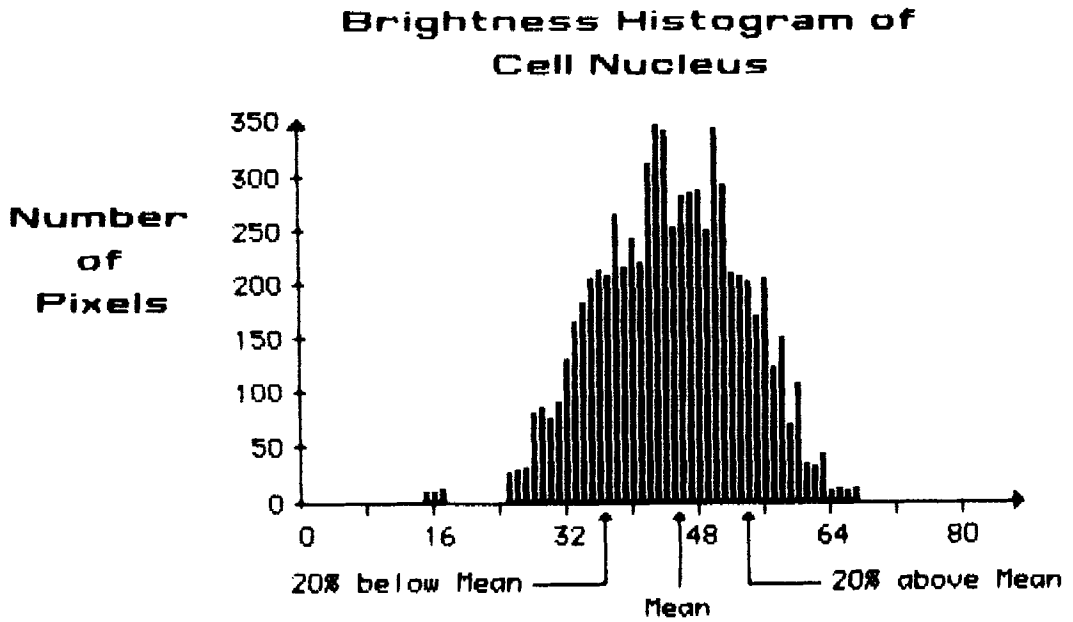


FIG. 3. Histogram of the cell nucleus shown in Figure 2A. Thresholds are automatically selected at 20 percent above and below the mean value of the nuclear brightness.

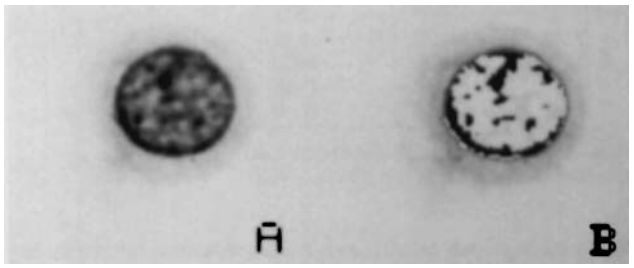


FIG. 4. Reassignment of the pixels in the bladder cell image according to Program 1. A) Original cell image; B) nucleus processed with percent = 20%.

ity measure is prefered over a heterogeneity measure, then we can simply define

$$\text{homogen} = 1 - \text{hetero} = \frac{N_G}{N_B + N_G + N_W}. \quad (2)$$

While the parameter *hetero* is quite capable of measuring the deviation from a uniform (i.e., homogeneous) chromatin distribution, it is not sensitive to the spatial distribution of the condensed chromatin. As the degree of granularity can play an important role in biological and clinical descriptions, separate measures are required.

Our measures for granularity return to the spatial distribution of the granularity as depicted in the labeled nucleus of Figure 4B. We look at the labeled nucleus through a mesh or sieve to determine the fraction of granules larger than the mesh size. We assume that the cells and their nuclei are randomly oriented and that there is no directional preference. Because of this, we replace the concept of a two-dimensional mesh with a one-dimensional mesh that operates along the rows of the nuclear image.

The choice of the mesh width is (again) a problem dependent issue. In our studies (9,23) we used a mesh that was 8 pixels (1 micrometer) wide. In a preparatory study (unpublished) we looked at the influence of various mesh sizes. We determined that, for the class of cells that we were interested in studying, a change in the mesh width of 25% produced little variation in the final results.

The mesh windows are non-overlapping. Within a given window we count the number of BLACK-labeled pixels and the number of WHITE-labeled pixels and take the absolute difference, *diff*. Only those mesh windows that fit totally within the nucleus "row" are used in the computation. This calculation is illustrated in Figure 5.

Based upon this sieving technique, two granularity measures may now be defined. The first measure, *clump*, reflects the size distribution of the granules and is given by:

$$\text{clump} = \frac{\Sigma_{\text{mesh}}\ \text{diff}}{N_B + N_W} \quad (3)$$

where $N_B$ and $N_W$, as defined earlier, are the total number of BLACK and WHITE labeled pixels in the nucleus, respectively. The sum is computed over all one-dimensional mesh windows. In Figure 5 there would be three such mesh windows. If $N_B = N_W = 0$, then *clump* is set to zero.

If the black and white pixels represent very fine gran-

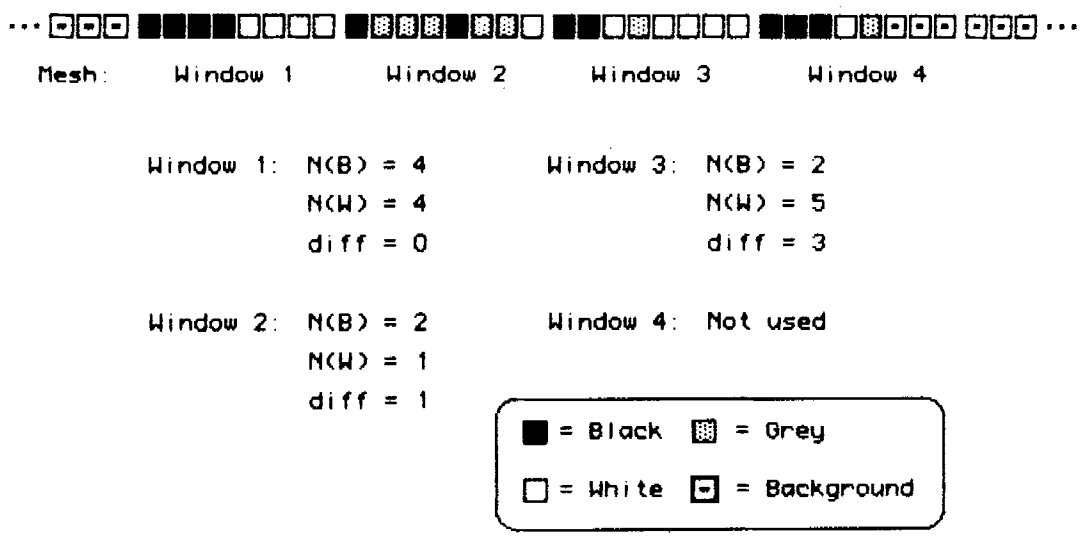


FIG. 5. One-dimensional sieve overlayed on a region containing nuclear pixels. The width of the mesh window in this example is eight pixels and the fourth window is not used because it contains non-nuclear pixels. The difference (*diff*) is defined as $diff = |N(B) - N(W)|$.

Table 1
*Values of Chromatin Parameters for Model Cells in Figure 2*[a]

| | | Hetero | Clump | Condens |
|---|---|---|---|---|
| Cell a | Normal nucleus | 0.20 | 0.93 | 0.19 |
| Cell b | Uniform optical density | 0.00 | 0.00 | 0.00 |
| Cell c | Large "granules" | 0.90 | 0.39 | 0.35 |
| Cell d | Small "granules" | 0.90 | 0.00 | 0.00 |

[a]The thresholds for labeling the cell nuclei were fixed at 20% above and below the mean (see Figure 3 and text). The mesh window was 8 pixels wide.

ulation, that is grains smaller than the mesh size, then the values of *diff* will be small and *clump* will be close to 0.0. If the granules are much larger than the mesh size then the values of *diff* will be large and *clump* will tend to 1.0.

The second measure, *condens*ation, reflects the fraction of large granules with respect to total nuclear area. The *condens*ation is defined by:

$$\text{condens} = \frac{\Sigma_{\text{mesh}}\ \text{diff}}{N_B + N_G + N_W}. \quad (4)$$

If all pixels in the nucleus are either BLACK or WHITE ($N_G = 0$) then *condens* will equal *clump*. In the more usual case, where some of the pixels are GREY then *condens* will take on a value somewhat less than *clump*. There exists an explicit relationship between these three parameters, *hetero*, *condens*, and *clump* given by:

$$\text{condens} = \text{clump} * \text{hereto}. \quad (5)$$

Since *clump* and hetero are both fractions between zero and one, we see immediately that:

$$0.0 \leqslant \text{condens} \leqslant \text{clump, hetero} \leqslant 1.0. \quad (6)$$

For the four model cells shown in Figure 2, the values of these chromatin distribution parameters are given in Table 1.

### Chromatin Condensation—Margination

Margination is that characteristic of chromatin distribution where the stained material is seen (in the two-dimensional image) "to collect" at the nuclear membrane. To form a measure, we return to the original grey-valued image. This image, as seen in Figure 4A, has been transformed by taking the logarithm of the original intensity image to yield an image where the value at every pixel in linearly related to the optical density of the stain at that pixel. For stoichiometrically stained cells this means that the sum of transformed image values in any subregion of the nucleus will be proportional to the stain content in that subregion. We assess the margination by computing the average opti-

cal density per pixel in a series of concentric "rings" that begin at the outside boundary and move inward toward the center of the nucleus. These rings are formed by beginning with the original nuclear contour and then considering the successive differences between the contour and its eroded versions. The Minkowski or cellular logic operation "erosion" is particularly suited to the development of this margination measure and can be effectively implemented in either hardware (3,15,17–19) or software (4,21). The procedure is illustrated in Figure 6 where the original cell and a graphic display of the rings are depicted.

Through this computation of the average optical density per pixel as a function of ring number, the radial spatial distribution of the optical density (that is, of nuclear stain) is determined. Thus, for the purposes of determining nuclear margination of stain, we reduce the two-dimensional distribution of stain to a one-dimensional radial profile m(r) as depicted in Figure 7. From this profile we then compute a second radial moment, a measure akin to (but not the same as) the radius of gyration. It is this scalar quantity that we use to describe the radial distribution of stained material.

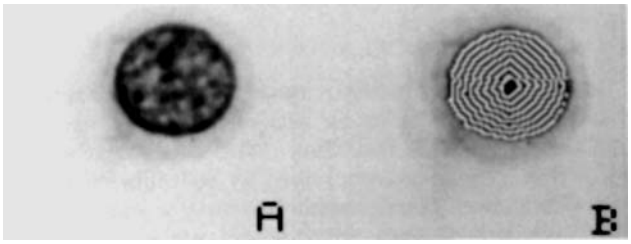


FIG. 6. Development and representation of the radial distribution of nuclear chromatin. A) Original cell showing nuclear margination; B) series of rings generated by erosions of the nuclear boundary. Notice that the ring shapes generated by erosions follow the nuclear shape.

To avoid confusion it is useful to point out that the definition of second moment that we use here differs subtly from the common definition found in college physics textbooks. We use a definition of m(r) based upon the average mass per pixel per ring. Thus, for a homogeneous object, m(r) is a constant for all r(ings). In classical mechanics a different quantity is defined. There, the mass distribution M(r) is the total mass in each ring. For a homogeneous object, M(r) therefore increases (linearly) as r increases. We have chosen the definition m(r) instead of M(r) because of the way it corresponds to the visual impression that the mass distribution in a homogeneous object is everywhere constant.

The second moment is given by (20):

$$I_2 = \frac{\int_0^R r^2\, m(r)\, dr}{\int_0^R m(r)\, dr} \tag{7}$$

where m(r) represents the average mass per pixel as a function of radial position r and R is the maximum radius. In our case, where the radii are replaced by ring numbers based upon erosions, equation 7 becomes:

$$I_2 = \frac{\sum_{r=0}^{R-1} r^2\, m(r)}{\sum_{r=0}^{R-1} m(r)} \tag{8}$$

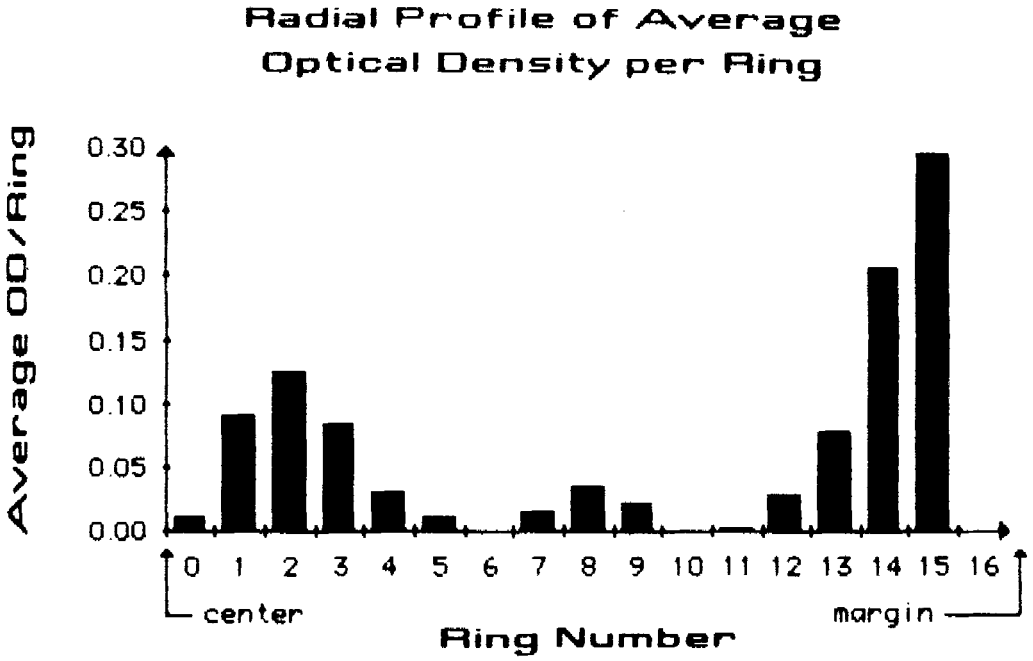


FIG. 7. Profile of the radial distribution of stained material from the nucleus shown in Figure 6.

and R is the maximum ring number, that is, the outer nuclear boundary. By examining two extreme cases we can determine a normalization for $I_2$. If all the mass is concentrated at the center of the nucleus then clearly $I_2 = 0.0$. If all the mass is concentrated at the edge of the nucleus—this can be modeled by $m(r) = M_0\,\delta(r-R)$—then $I_2 = R^2$. We therefore define nuclear margination, *marg*, as:

$$\text{marg} = I_2/R^2 \tag{9}$$

and, in general, $0.0 \leqslant \text{marg} \leqslant 1.0$. For a nucleus with uniformly distributed chromatin, where the histogram in Figure 7 is flat between 0 and R, the value of *marg* is given by

$$\text{marg} = (1/3) - (1/2)\,R^{-1} + (1/6)R^{-2}. \tag{10}$$

The discrete nature of the calculation is apparent in equation 10. In the continuous case the answer would be ⅓ and as the radius of the nucleus becomes large (with respect to the picture sampling density) this is the case. The difference between the value ⅓ and the result in eq. 10 is simply the quantization error associated with the discrete, spatial sampling grid.

Based upon this quantization error it is straightforward to derive a relationship between the image sampling density—as expressed by R—and the percentage error in the estimate of *marg*. We can define the percentage error (e%) for the homogeneous object as:

$$e\% = \frac{|1/3 - \text{marg}|}{1/3} \times 100\%, \tag{11}$$

that is, the normalized difference between the "true" analog value and the estimated digital value. If we require that e% be below a certain threshold, say p%, and we ignore terms on the order of $R^{-2}$, then using equation (10) this result can be rewritten as:

$$R > \frac{300}{2p}. \tag{12}$$

Thus, if the percentage quantization error is to be below $p = 2\%$, then it is necessary to choose a sampling density in the original image such that the nuclear radius is at least 75 pixels! For a nucleus approximately 10 micrometers in diameter this would imply a sampling density of at least 15 pixels per micrometer.

## Preprocessing for Measurement

**Sampling density.** Before the four chromatin features can be measured a number of preprocessing steps are necessary. First, and perhaps most frequently underestimated, is the importance of choosing a proper sampling density. As we have just shown, the quantization error associated with the choice of sampling density can be of significant size. In the results that we will be presenting shortly the cell images were sampled at a density of 8 pixels per micrometer and the nuclei were approximately 5 micrometer in diameter. Based upon our results from the previous section it would not have been unreasonable to use a sampling density of 16 pixels per micrometer or greater to minimize the errors due to spatial quantization. In fact, in several different studies, including one of ours on the quantification of shape changes in mammalian sperm, sampling densities of from 16 to 30 pixels per micrometer have been reported (6,22). The choice of sampling density couples, of course, to our measure of chromatin granularity. At a sampling density of 8 pixels per micrometer and with a mesh window of 8 pixels, we are sieving for granules of 1 micrometer diameter. Should we choose a higher sampling density then a wider mesh (in pixels) would be necessary to maintain a constant size relative to the granules.

**Segmentation of nuclear image.** All of our chromatin measures depend upon an accurate assessment of the nuclear/cytoplasmic boundary. With a proper choice of stain this may be accomplished by ordinary thresholding. When special circumstances arise (for example with phase or interference microscopy) more complicated techniques may be required to delineate the boundary, for example heuristic search techniques. One must remain mindful, however, of the computational complexity of such algorithms and how they can limit or at least affect total cell analysis throughput (13).

**Contour encoding and processing.** All of the chromatin measures described here have been implemented using the "run table" formulation described in reference 21. This has led to an efficient and thus rapid code [in the C programming language (8)] for acquiring the pixels within the nucleus, histograms within a specific region or ring, and the implementation of erosions and other binary operators. Two optional pre-processing steps that can be used for the chromatin measures are a pre-erosion of the nuclear contour before the measurement of *hetero*, *clump*, and *condens* and a pre-dilation of the nuclear contour before the measurement of *marg*. Both optional steps are useful when there is an uncertainty about the exact position of the nuclear boundary. In both cases the pre-processing of either erosion or dilation produces a border that more conservatively estimates the boundary with respect to the desired measure(s). The number of pre-processing erosion or dilation steps is a function of the sampling density and the electro-optical transfer function of the measuring system. In our case this turned out to be two pre-erosions of the nuclear contour for the heterogeneity and granularity measures and zero pre-dilations for the margination measure.

## RESULTS

The ultimate test of any measure is, of course, how well it works in describing the similarities within cell populations and the differences between cell populations. In two very different sets of experiments the chromatin measures described here were used along with other conventional measures such as nuclear area, nuclear optical density, cytoplasmic area size, etc. to characterize populations of cells. Since both experiments are described in detail elsewhere (9,23) only the issues relevant to assessing the utility of our chromatin measures will be presented here.

In the first experiment (23) a population of rats was exposed to a known carcinogen to produce bladder cancer. The morphology of dissociated urothelial cells was compared against those from a control population. Samples were taken up to 45 weeks after onset of exposure and a visually distinct change in the nuclear chromatin pattern appeared as the weeks progressed (10). The ACUity system (22) was used to scan samples and to measure various parameters including nuclear area, nuclear area/cytoplasmic area (N/C) ratio, and the chromatin distribution measures. A set of abnormal cells (as determined by a cytotechnologist) from the exposed animals was compared against a randomly selected set of control cells using the non-parametric Mann-Whitney ranks test [BMDP test, P3S (7)]. The nuclear area was significantly larger at the 14, 34, and 45 week time points (after birth) with p values of 0.05, 0.146, and 0.0037, respectively. There was no significant difference in nuclear area at 26 weeks. N/C ratio showed low discriminatory power although the same general trends noted in nuclear area were also present.

The chromatin parameters differed significantly between test and control cells (animals) at all time points. Abnormal cells had chromatin that was more heterogeneous with greater condensation (larger clumps). The levels of significance (.0001, .05, .0001, .0001 at 14, 26, 34, and 45 weeks, respectively) were significantly better than those for nuclear area and, in fact, all other parameters measured. Further, these results were consistent with the cytopathologist's verbal description of increased chromatin condensation in abnormal cells.

In the second experiment (9) images of foam cells in human nipple aspirate fluid were analyzed with the ACUity system in a study to attempt to distinguish among cases diagnosed as benign, hyperplasia, atypical hyperplasia, and cancer. A total of 23 cell parameters were measured on the nuclear and cytoplasmic portions of the images of 331 cells. Among the 11 parameters selected for high discriminatory power ($p < 0.005$) were our four chromatin measures: *hetero, condens, clump,* and *marg*. When linear, stepwise discriminant analysis was applied to determine the best set of three parameters for separating the four groups (benign through cancer), heterogeneity, margination, and average nuclear stain were selected. When individual cases were considered, (there were 12 individual cases over the four groups), the chromatin texture parameters proved the most powerful in classifying the individual cases. Once again these results follow the observation of the cytopathologist that change in chromatin is considered to be the most reliable feature for recognition of neoplasia and preneoplasia in clinical cytology.

## SUMMARY AND CONCLUSIONS

Several research groups have recognized and implemented parameters for the description of chromatin texture that are oriented more towards the descriptions of the cell nucleus (or cytoplasm) and less towards an *ad hoc* mathematical formalism. These include the counting densitogram [Bins et al. (1)], which estimates the number of dark and light regions inside a cell nucleus and the similar numbers for cell cytoplasm. Landeweerd (12) also devised a technique for labeling a nuclear image with three levels. His final measures based upon the labeled image were somewhat different from ours and no simple explanation was presented for the relation between the parameters and the changes occuring during chromatin condensation. Krans et al., in their paper (11) on discrimination of normal and dyskaryotic cells, offer in their Figure 3 a concept quite similar to that shown in our Figure 2. Their method of assessing the granulation seems to differ significantly, however. Nowhere in the literature does there appear to be an attempt to quantify the concept of nuclear margination.

In this paper we have presented four measures for the quantitative description of nuclear chromatin texture. These measures satisfy four important requirements for quantitative pathology. First, the measures can be described and related to changes in nuclear appearance, changes that correlate with the descriptions used by cytopathologists. Second, we understand how the measures change as the chromatin becomes more clumped (clump tends to 1.0), more marginated (marg tends to 1.0), etc. Third, as was demonstrated through several experiments, the measures perform well both in the empirical sense and also in comparison with other conventional morphological parameters. Fourth, the measures can be rapidly measured as their structure admits an efficient algorithmic implementation.

In summary, we believe that the four chromatin measures provide important new tools for image cytometry and its application in biomedical research and clinical diagnosis.

## ACKNOWLEDGMENTS

We would like to acknowledge the advice and help of our colleagues Dr. Martin Vanderlaan, Dr. Eileen King, Ms. Lois Kromhout, and Ms. Abby Grover. This work was partially supported by the grants from the National Cancer Institute, Grant Number CA-28833, the National Bladder Cancer Project, Grant Number CA-23790, the U.S. Department of Energy contract with the Lawrence Livermore National Laboratory number W-7405-ENG-48, and the Praeventie Fonds.

## LITERATURE CITED

1. Bins M, Landeweerd GH, Gelsema ES, van Montfort LH, Halie MR: Texture of white blood cells expressed by the counting densitigram. Cytometry Vol. 1:321–324, 1981.

2. Galloway, MM: Texture analysis using gray level run lengths. Comput Graphics Image Process 4:172–179, 1975.
3. Gerritsen FA, and Aardema LG: Design and use of DIP-1: A fast, flexible and dynamically microprogrammable pipelined image processor. Pattern Recognition 14:319–330, 1981.
4. Groen FCA, and Foster NJ: A fast algorithm for cellular logic operations on sequential machines. Pattern Recognition Letters 2:333–338, 1984.
5. Haralick RM, Shanmugan K, Dinstein I: Textural features for image classification. IEEE Trans. on Systems, Man, and Cybernetics, Vol. SMC-3:610–621, 1973.
6. Harms H, and Aus HM: Estimating the sampling error in a high resolution TV microscope image processing system. Cytometry 5:228–235, 1984.
7. Hill M,: BMDP User's Digest: A Condensed Guide to the BMDP Computer Programs. BMDP Statistical Software, Dept. of Biomathematics, UCLA, 1979.
8. Kernighan BW, and Ritchie DM: The C Programming Language. Prentice-Hall, Englewood Cliffs, N.J., 1978.
9. King EB, Kromhout LK, Chew KL, Mayall BH, Petrakis NL, Jensen RH, Young IT: Analytical studies of foam cells from breast cancer precursors. Cytometry 5:124–130, 1984.
10. King EB, Vanderlaan M, Jensen RH, Kromhout LK, Hoffman JW: Morphologic changes in rat urothelial cells during carcinogenesis. I: Histologic and cytologic changes. Cytometry 5:447–453, 1984.
11. Kraus H, Schwarz J, Neumann GK: Discrimination of normal and diskaryotic cells with a new high-resolution system (CIALIS). Anal Quant Cytol 5:28–30, 1983.
12. Landeweerd GH: Pattern recognition of white blood cells. Doctoral dissertation, Vrije Universiteit te Amsterdam, October, pp 79–87, 1981.
13. Lester J, Williams H, Weintraub B, Brenner J: Two graph searching techniques for boundary finding in white blood cell images. Comput Biol Med 8:293–308, 1978.
14. Herman CJ, personal communication.
15. Meyer F: Iterative image transformations for an automatic screening of cervical cancer. J Histochem Cytochem 27:128–135, 1979.
16. Pressman NJ: Optical texture analysis for automatic cytology and histology: A Markovian approach. Lawrence Livermore Laboratory Report UCRL-52155, October, 1976.
17. Preston K: Feature extraction by golay hexagonal pattern transformations. IEEE Trans. on Computers, Vol. C-20:1007–1014, 1971.
18. Serra J: Image analysis and Mathematical Morphology. Academic Press, London 1982.
19. Sternberg S: Language and Architecture for Parallel Image Processing. Proc. Pattern Recognition in Practice. North Holland, The Netherlands, 1980.
20. Thomas GB: Calculus and Analytic Geometry. Addison-Wesley, Reading, Massachusetts, 1960.
21. Young IT, Perverini RL, Verbeek PW, van Otterloo PJ: A new implementation for the binary and Minkowski operators. Comput Graphics Image Process 17:189–210, 1981.
22. Young IT, Gledhill BL, Lake S, Wyrobek AJ: Quantitative analysis of radiation-induced changes in sperm morphology. Anal Quant Cytol 4:207–216, 1982.
23. Young IT, Vanderlaan M, Kromhout LK, Jensen RH, Grover A, King EB: Morphologic changes in rat urothelial cells during carcinogenesis. II: Image Cytometry. Cytometry 5:454–462, 1984.